Enhanced Global Digital Image Correlation for Accurate Measurement of Microbeam Bending

L. I. J. C. Bergers, J. Neggers, M. G. D. Geers and J. P. M. Hoefnagels

1 Introduction

Microbeams are simple on-chip test structures used for thin film and MEMS materials characterization [3], see Fig. 1. Optical profilometry techniques are typically used for the measurement of deformations [8, 10]. Profilometry can be combined with Euler-Bernoulli (EB) beam theory to extract material parameters, like the E-modulus or creep parameters. The latter requires characterization of time-dependent microbeam bending, though non-trivial, as it involves long term sub-microscale measurements. On the one hand environmental instabilities directly hinder accurate long term measurements. On the other hand microfabrication limitations often affect the ideal fixed-end geometrical boundary condition [2]. This requires attention, because a non-ideal fixed-end, e.g. a compliant anchor, introduces errors when using the microbeam *deflection* with EB-theory [6]. Hence, the problem is attaining sufficient accuracy and precision in these measurements.

A first step towards precise microbeam bending experiments is the careful design and construction of the setup and proper control of the profilometer's environment [1]. In [1] we presented a simple image correlation based methodology to correct the rigid body motions, e.g. due to drift, of the deformed specimen on the $xy\theta_x\theta_y$-positioning stage. The difference between the reference profile and this deformed profile yielded the tip deflection. However, this correlation based correction has a drawback: the correction is extrapolated to the entire beam profile based on a limited

L. I. J. C. Bergers · J. Neggers · M. G. D. Geers · J. P. M. Hoefnagels (✉)
Department of Mechanical Engineering, Materials Technology,
Eindhoven University of Technology, P.O. Box 513, 5600 MB Eindhoven, The Netherlands
e-mail: j.p.m.hoefnagels@tue.nl

L. I. J. C. Bergers
Foundation for Fundamental Research on Matter, P.O. Box 3021, 3502 GA Utrecht,
The Netherlands

L. I. J. C. Bergers
Materials innovation institute M2i, P.O. Box 5008, 2600 GA Delft, The Netherlands

H. Altenbach and S. Kruch (eds.), *Advanced Materials Modelling for Structures*,
Advanced Structured Materials 19, DOI: 10.1007/978-3-642-35167-9_5,

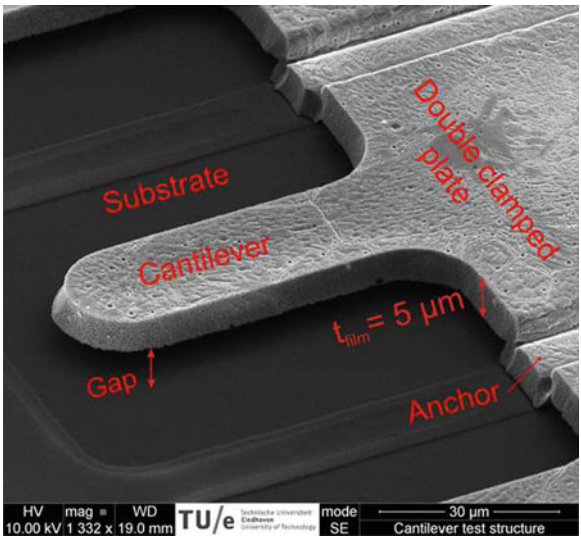

Fig. 1 Scanning electron micrograph of a typical on-chip microbeam attached to a free-standing double clamped plate that is anchored to the substrate

reference area on the anchor. As the beam lies in the extended direction of the anchor, the resulting tip deflection is sensitive to an extrapolation error.

Following Neggers et al. [7], we here present an improved approach for microbeam bending analysis. The approach in [7] extracts curvature from profilometry data of bulged membranes through enhanced global digital image correlation (GDIC). The key point is the use of the deformation kinematics as degrees of freedom to be solved in the minimization problem formulated for DIC as demonstrated by Hild and Roux [4, 5]. Therefore, in the approach presented here we combine the drift and beam bending kinematics and directly correlate on the beam, eliminating any extrapolation errors. The correlation procedure yields the displacement fields. This does not directly yield the beam *deflection*, because the position of the anchor is not resolved. However, the *curvature* field of the beam can be directly extracted from this displacement field, because a C2-continuous basis for the degrees of freedom is chosen. This effectively filters measurement noise, overcoming issues when taking derivatives to calculate the curvature. In short, this improved approach yields an accurate curvature field, in stead of beam deflection, that serves equally well in analyzing microbeam bending mechanics.

In this work, we describe the kinematics involved followed by the implementation into the GDIC procedure through which the curvature is determined. To asses the accuracy of this new procedure a numerical experiment is performed of which the implementation and results are discussed.

2 Principle of Global Digital Image Correlation and Curvature Measurement

In the solid mechanics community DIC has become an established method to measure deformation fields at various length scales both in 2D and 3D geometries [9]. For the 2D case one records an image of an undeformed, reference situation of an object and of its the deformed situation. Parts of the image with a unique pattern can then be correlated from one image to the next, allowing one to extract the displacements between the two instances. Traditionally, one applies a pattern with sufficient detail and variation to obtain uniqueness for the correlation procedure.

The correlation procedure in 2D is based on the principle of optical flow conservation. It states that the reference image, represented by the intensity field $f(\mathbf{x})$, is related to the deformed image, $g(\mathbf{x})$ through the in-plane displacement field $\mathbf{u}_{xy}(\mathbf{x})$ and measurement noise $n_0(\mathbf{x})$:

$$g(\mathbf{x} + \mathbf{u}_{xy}(\mathbf{x})) = f(\mathbf{x}) + n_0(\mathbf{x}). \tag{1}$$

In the case of optical profilometer data, the intensity is in fact a height, and can also vary due to e.g. deformations. This quasi 3D nature can be exploited by relaxing the optical flow conservation:

$$g(\mathbf{x} + \mathbf{u}_{xy}(\mathbf{x})) = f(\mathbf{x}) + u_z(\mathbf{x}) + n_0(\mathbf{x}). \tag{2}$$

The unknown displacement fields $\mathbf{u}(\mathbf{x})$ are found through minimizing the global residual η of the weak form of Eq. (2) over the considered domain

$$\eta^2 = \int [(f(\mathbf{x}) - g(\mathbf{x} + \mathbf{u}_{xy}(\mathbf{x})) + u_z(\mathbf{x})]^2 d\mathbf{x} = \int r(\mathbf{x})^2 d\mathbf{x}, \tag{3}$$

where $r(\mathbf{x})$ is the residual field. The displacement field is parameterized and interpolated using a set of basis functions $\phi_n(\mathbf{x})$ acting globally over the entire domain and weighted with a discrete set of degrees of freedom u_n

$$\mathbf{u}(\mathbf{x}) = u_x(\mathbf{x})\mathbf{e}_x + u_y(\mathbf{x})\mathbf{e}_y + u_z(\mathbf{x})\mathbf{e}_z = \sum_n u_n \phi_n(\mathbf{x})\mathbf{e}_i, \tag{4}$$

where $i = [x, y, z]$ and the basis functions $\phi_n(\mathbf{x})$ are polynomial functions depending on $\mathbf{x} = x\mathbf{e}_x + y\mathbf{e}_y$

$$\phi_n = x^{\alpha(n)} y^{\beta(n)}. \tag{5}$$

The choice for this parametrization has the benefit that it allows one to introduce degrees of freedom suitable for describing the deformation kinematics, whilst maintaining a continuously differentiable solution. This aspect is important, because the strain and, particularly for microbeam bending, curvature fields are (higher order)

derivatives of the displacement fields. Furthermore when the order of the polynomials are limited, measurement noise is effectively filtered, yielding a robust curvature measurement: the smooth continuously differentiable displacement fields and not the measurement data serve as input for differentiation.

The introduction of the degrees of freedom and the appropriate basis functions can be based on prior knowledge of the deformation kinematics. For example, a uniaxial strain in x, ϵ_{xx}, could be described by adding a basis function of degree $[\alpha, \beta] = [1, 0]$ in x-direction: $\phi_{10} = x^1 y^0$. Adding this basis function to the z-direction would describe a constant tilt. One should however be aware that superfluous degrees of freedom will not necessarily yield the correct solution for the displacement fields, because of the measurement noise. On the other hand residual fields showing systematic deviations from zero might indicate insufficient kinematic degrees of freedom. Therefore, the prior knowledge allows a sufficient choice of degrees of freedom that will describe the kinematics, but limit inaccuracies due to noise.

As the curvature field is the desired measurand from the microbeam bending experiment, we consider all rigid body displacements, rotations about the x- and y-axis, resulting from drift of the $xy\theta_x\theta_y$-platform, and the end-loaded bending of the single clamped microbeam. The bending results in a gradient in curvature, involving a third order displacement derivative along the beam's axis, which is taken along the x-direction. Hence the parametrization of the displacement fields takes the following form:

$$u(x) = (u_{x,00})\mathbf{e}_x + (u_{y,00})\mathbf{e}_y + (u_{z,00} + u_{z,10}x + u_{z,01}y + u_{z,20}x^2 + u_{z,30}x^3)\mathbf{e}_z. \quad (6)$$

From the displacement fields resulting from the GDIC procedure, the curvature field tangent to the beam's surface in x-direction, $\kappa_{xx}(\mathbf{x})$, can be derived. First the curvature tensor is constructed as the dyadic product of the gradient operator and the surface normal:

$$\kappa = \nabla \otimes \mathbf{n}, \quad (7)$$

where the gradient operator is defined as

$$\nabla = \mathbf{e}_x \frac{\partial}{\partial x} + \mathbf{e}_y \frac{\partial}{\partial y} + \mathbf{e}_z \frac{\partial}{\partial z}. \quad (8)$$

The normal vector is calculated from the position field of the deformed microbeam $z(x, y)$, obtained by applying the resulting displacement fields to the reference profile:

$$\mathbf{n} = \frac{\nabla z(\mathbf{x})}{||\nabla z(\mathbf{x})||}. \quad (9)$$

Finally the curvature field in a given tangent direction is calculated by

$$\kappa_{\mathbf{t}}(\mathbf{x}) = \mathbf{t} \cdot \kappa \cdot \mathbf{t} \quad (10)$$

where the unit tangent vector, $\mathbf{t}(\boldsymbol{\tau})$, along an in-plane unit vector $\boldsymbol{\tau}(\mathbf{x}) = \tau_x \mathbf{e}_x + \tau_y \mathbf{e}_y$ is

$$\mathbf{t} = \frac{\tau_x \mathbf{e}_x + \tau_y \mathbf{e}_y + (\nabla f) \cdot \boldsymbol{\tau} \otimes \mathbf{e}_z}{\sqrt{{\tau_x}^2 + {\tau_y}^2 + [(\nabla f) \cdot \boldsymbol{\tau}]^2}} \tag{11}$$

and $\boldsymbol{\tau} \otimes \mathbf{e}_z$ is the dyadic product of the two vectors. In the processing applied, the curvature is measured along the tangent in-plane unit vector $\boldsymbol{\tau} = 1\mathbf{e}_x$.

3 Evaluation of Accuracy

In order to evaluate the accuracy of the GDIC approach a numerical microbeam bending experiment is conducted. A linear elastic finite element model of a representative microbeam ($l = 100$ µm, $w = 20$ µm, $t = 5$ µm) is modeled in Marc/Mentat using quadratic thick shell elements, see Fig. 2. Only half of the microbeam is modeled due to symmetry. It is deflected at the end by 2 µm. The surface topography of a physical microbeam is measured using a Sensofar Plu2300 confocal optical profilometer, see Fig. 3a and [1] for details. A corresponding part of this topography, see ROI_f in Fig. 3b, is deformed with the numerically generated displacement fields. An additional constant in-plane displacement $\mathbf{u}_{xy}(\mathbf{x}) = 1,162\mathbf{e}_x - 0,830\mathbf{e}_y$ µm as well as an out-of-plane tilt $\mathbf{u}_z(\mathbf{x}) = (0,0005x - 0,0006y)\mathbf{e}_z$ µm simulate drift, see ROI_g in Fig. 3b. These values are selected as uneven half-pixel multiples, where the pixel size is $0,332 \times 0,332$ µm^2, serving as a worst case, because this leads to the poorest DIC accuracy [4]. The deformed and displaced topography serves as input for the GDIC procedure with the natural surface features serving as the pattern. Subsequently the curvature is calculated based on the GDIC output and compared to the numerically prescribed curvature calculated from the nodal displacements and rotations of the FEM output.

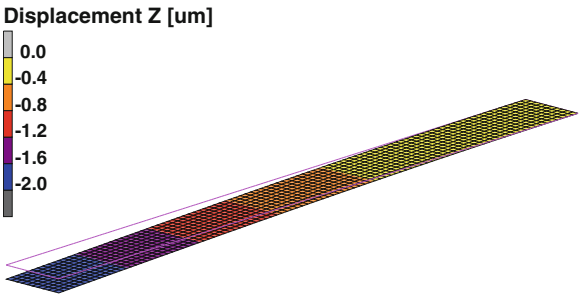

Fig. 2 The FEM model in deformed state used for generating the displacement fields. The left end is deflected, whilst the right end is clamped

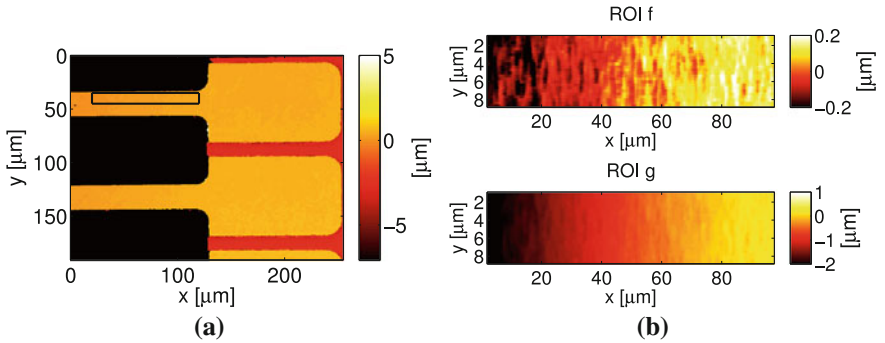

Fig. 3 **a** A contour plot of two actual microbeams. The box on the top beam's surface indicates the part used for GDIC as shown in **b**: ROIs of the undeformed **f** and deformed **g** selection from the beam

To minimize numerical artifacts when doing this numerical evaluation there are some issues to address. First, the computational mesh and discrete surface topography will have a different discretization. This is overcome by interpolating both surfaces with C1- or C2-continuous interpolation functions to finer and equal grids and excluding pixels adjacent to the border of the region of interest. Second, the prescribed curvature fields calculated from interpolated nodal displacement fields will show artifacts, because the nodal displacements are not C1-continuous between elements. Although nodal rotations strictly speaking also suffer the same discontinuity, they effectively do form a C1-continuous gradient of the displacement field for the curvature calculation. Hence the nodal rotations θ_i are interpolated and used in the curvature calculation through the following definition of $\mathbf{n}$:

$$\mathbf{n} = \frac{\tan(\theta_y(\mathbf{x}))\mathbf{e}_x + \tan(\theta_x(\mathbf{x}))\mathbf{e}_y + \mathbf{e}_z}{\sqrt{\tan(\theta_x(\mathbf{x}))^2 + \tan(\theta_y(\mathbf{x}))^2 + 1}}. \tag{12}$$

4 Results

The results of the GDIC at different levels of deflection are judged by the displacement fields obtained in x-, y- and z-direction and the residual field. The resulting displacement fields show good agreement with the prescribed displacement fields, see Fig. 4. For the in-plane displacements an accuracy of <13 nm is observed, which corresponds to $\sim$0, 04 pixels for a 332 nm pixel size. The accuracy of the z displacement field is <2 nm, whilst its field reveals a systematic error. This might be caused by a slight curvature in y-direction that is not covered by the admitted degrees of freedom.

When regarding the residual field and comparing to the undeformed pattern, see Fig. 5, no systematic features are observed, indicating the correlation has reached the

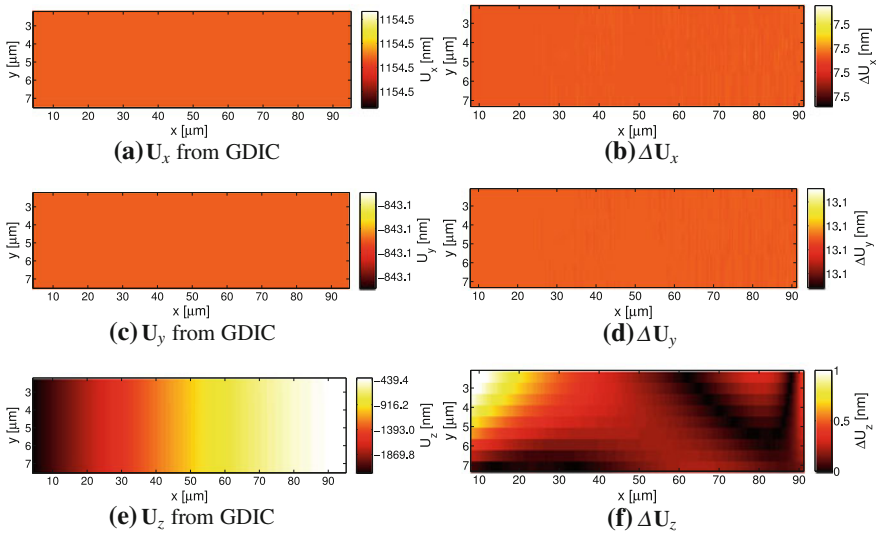

Fig. 4 Resulting displacement fields including drift at 2 µm deflection obtained through GDIC. **a, c, e** are the GDIC obtained displacement fields and **b, d, f** are the difference fields between the GDIC and FEM displacement fields

global minimum. Further, the amplitude of the residual field is relatively large, about 10 % of the undeformed pattern. If the global minimum is obtained, this amplitude can only be attributed to the limited number of pixels, being $\sim 20 \times 190$, and the effect of interpolating the surface pattern within the correlation algorithm. Improving this requires a smoother surface pattern and higher spatial sampling. Nonetheless, the results are adequate compared to local DIC approaches where typically facets of 15×15 pixels are employed to resolve displacement fields with similar accuracy.

The curvature fields κ_{xx} obtained through the GDIC at 1 and 2 µm deflection and the difference between these and the simulated κ_{xx} reveal a good measurement of κ_{xx}, see Fig. 6. The expected gradient in κ_{xx} is visible, approaching 0 at the tip of the beam (left hand side of images) and reaching a maximum at the clamped end (right hand side of images). The difference shows a limited error, caused by the limited choice of degrees of freedom and required interpolation during correlation.

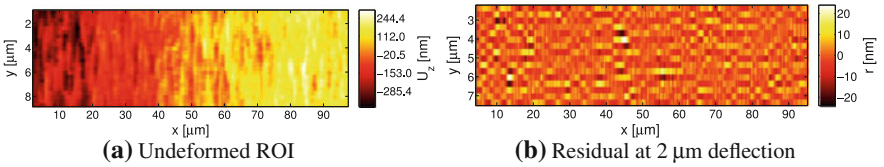

Fig. 5 Comparison of the amplitude in the pattern and the resulting residuals showing a relatively low residual

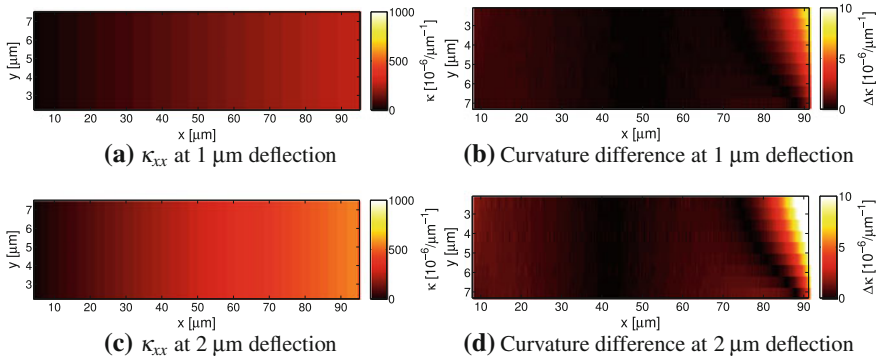

(a) κ_{xx} at 1 µm deflection **(b)** Curvature difference at 1 µm deflection

(c) κ_{xx} at 2 µm deflection **(d)** Curvature difference at 2 µm deflection

Fig. 6 Curvature fields κ_{xx} at 1 and 2 µm deflection reveal the expected gradient, whilst the differences with the numerically prescribed fields show a good accuracy

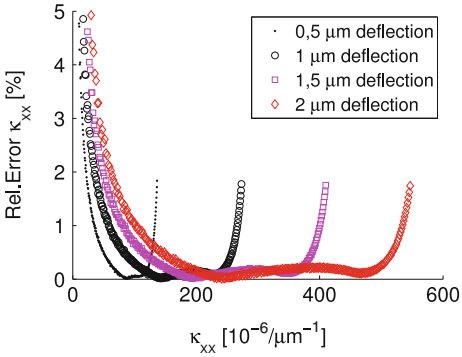

Fig. 7 The accuracy of κ_{xx} obtained is good for the part of the ROI that is not near the loaded end or the clamped end

Within the probed range of κ_{xx} the accuracy of the measurement is $<1\,\%$ for most of the ROI, see Fig. 7. The accuracy, defined as the relative error $(\kappa_{xx,GDIC} - \kappa_{xx,FEM})/\kappa_{xx,FEM}$, increases near the clamped end due to the additional κ_{yy} and at the loaded end due to the definition of the accuracy. Naturally one can opt not to measure data near these regions.

5 Conclusion

We presented an enhanced digital image correlation approach to extract beam curvature from full-field deformation data of microbeam bending experiments. A limited yet sufficient amount of degrees of freedom in the GDIC described the bending kinematics as well as possible rigid body motions that might be caused due to drift in actual experiments. A numerical analysis of the accuracy based on FEM revealed that the proposed GDIC accurately resolved the bending kinematics: an accuracy in the κ_{xx}-measurement of $<1\,\%$ for parts of the beam away from the clamped and free

ends. The presented numeric analysis can also be extended to simulate the influence of measurement artifacts, e.g. noise or pattern quality. This GDIC methodology thus enables the precise measurement of beam curvature required for time-dependent microbeam bending experiments. It might also find application in other microbeam bending analyses, e.g. stress measurements of deflecting structural parts of microdevices in case of known material parameters.

Acknowledgments This research was carried out under Project number M62.2.08SDMP12 in the framework of the Industrial Partnership Program on Size Dependent Material Properties of the Materials innovation institute M2i (http://www.m2i.nl) and the Foundation of Fundamental Research on Matter (FOM), which is part of the Netherlands Organization for Scientific Research (NWO).

References

1. Bergers, L.I.J.C., Hoefnagels, J.P.M., Delhey, N.K.R., Geers, M.G.D.: Measuring time-dependent deformations in metallic MEMS. Microelectron. Reliab. **51**, 1054–1059 (2011)
2. Gill, J.J.Y., Ngo, L.V., Nelson, P.R., Kim, C.J.: Elimination of extra spring effect at the step-up anchor of surface-micromachined structure. J. Microelectromech. Syst. **7**, 114–121 (1998)
3. Guckel, H., Burns, D., Rutigliano, C., Lovell, E., Choi, B.: Diagnostic microstructures for the measurement of intrinsic strain in thin films. J. Micromech. Microeng. **2**, 86–95 (1992)
4. Hild, F., Roux, S.: Digital image correlation: from displacement measurement to identification of elastic properties—A review. Strain **2**, 69–80 (2006)
5. Hild, F., Roux, S.: Comparison of local and global approaches to digital image correlation. Exp. Mech. **52**(9), 1503–1519 (2012). doi:10.1007/s1134001296037
6. Menčík, J., Quandt, E.: Determination of elastic modulus of thin films and small specimens using beam bending methods. J. Mater. Res. **14**, 2152–2161 (1999)
7. Neggers, J., Hoefnagels, J.P.M., Hild, F., Roux, S., Geers, M.G.D.: A Global Digital Image Correlation enhanced full-field bulge test method. Proc. IUTAM. **4**, 73–81 (2012)
8. O'Mahony, C., Hill, M., Brunet, M., Duane, R., Mathewson, A.: Characterization of micromechanical structures using white-light interferometry. Meas. Sci. Tech. **14**, 1807–1814 (2003)
9. Sutton, M.A., Orteu, J., Schreier, H.W.: Image Correlation for Shape. Motion and Deformation Measurements. Springer, New York (2009)
10. Van Spengen, W.M., Puers, R., Mertens, R., De Wolf, I.: Characterization and failure analysis of MEMS: high resolution optical investigation of small out-of-plane movements and fast vibrations. Microsyst. Technol. **10**, 89–96 (2004)